Phosphocode-dependent functional dichotomy of a common co-receptor in plant signaling

Artemis Perraki[1,5], **Thomas A. DeFalco**[1,2], **Paul Derbyshire**[1], **Julian Avila**[3,4,6], **David Séré**[1,7], **Jan Sklenar**[1], **Xingyun Qi**[3,4], **Lena Stransfeld**[1,2], **Benjamin Schwessinger**[1,8], **Yasuhiro Kadota**[1,9], **Alberto P. Macho**[1,10], **Shushu Jiang**[1,11], **Daniel Couto**[1,12], **Keiko U. Torii**[3,4], **Frank L.H. Menke**[1], and **Cyril Zipfel**[1,2,*]

[1]The Sainsbury Laboratory, Norwich Research Park, Norwich, UK. [2]Institute of Plant and Microbial Biology and Zürich-Basel Plant Science Center, University of Zürich, Zürich, 8008, Switzerland. [3]Howard Hughes Medical Institute, University of Washington, Seattle, USA. [4]Department of Biology, University of Washington, Seattle, USA. [5]Present address: Department of Plant Sciences, University of Cambridge, CB2 3EA, UK. [6]Present address: Metabolomics Platform, the Broad Institute, Cambridge, MA 02142 USA. [7]Present address: Laboratoire de Biochimie et Physiologie Moléculaire des Plantes, Institut de Biologie Intégrative des Plantes 'Claude Grignon', UMR CNRS/INRA/SupAgro/UM2, Place Viala, 34060 Montpellier cedex, France. [8]Present address: The Australian National University, Research School of Biology, Acton ACT 2601, Australia. [9]Present address: RIKEN Center for Sustainable Resource Science, Suehiro-cho 1-7-22 Tsurumi-ku, Yokohama 230-0045, Japan. [10]Present address: Shanghai Center for Plant Stress Biology, CAS Center for Excellence in Molecular Plant Sciences; Shanghai Institutes of Biological Sciences, Chinese Academy of Sciences, Shanghai 201602, China. [11]Present address: Institute of Biochemistry and Cell Biology, Shanghai Institutes for Biological Sciences, Chinese Academy of Sciences. [12]Present address: Department of Botany and Plant Biology, University of Geneva, Switzerland.

Abstract

Multicellular organisms employ cell-surface receptor kinases (RKs) to sense and process extracellular signals. Many plant RKs form ligand-induced complexes with shape-complementary co-receptors for their activation[1]. The best-characterized co-receptor is BRASSINOSTEROID INSENSITIVE 1-ASSOCIATED KINASE 1 (BAK1), which associates with numerous leucine-rich repeat (LRR)-RKs to control immunity, growth, and development[2]. Here, we report key regulatory events controlling the functionality of BAK1 and, more generally, LRR-RKs. Through a combination of phospho-proteomics and targeted mutagenesis, we identified conserved phosphosites that are required for BAK1 immune function in *Arabidopsis thaliana* (hereafter Arabidopsis). Strikingly, these phosphosites are not required for BAK1-dependent brassinosteroid (BR)-regulated growth. In addition to revealing a critical role for BAK1 C-terminal tail phosphorylation, we identified a conserved tyrosine phosphosite that may be required for functionality of the majority of Arabidopsis LRR-RKs, and separates them into two distinct functional classes. Our results suggest a phosphocode-based dichotomy of BAK1 functionality in plant signaling, and provide novel insights into receptor kinase activation, which have broad implications for our understanding of how plants respond to their changing environment.

RKs control all aspects of plant life, ranging from development to stress response, and depend on ligand-induced interaction with co-receptors for receptor activation[1]. In particular, plant LRR-RKs often form complexes with short, shape-complementary co-receptors of the SOMATIC-EMBRYOGENESIS RECEPTOR KINASE (SERK) family[2]. Arabidopsis SERK3 (also named BAK1) is the best-characterized member of this family, and forms ligand-induced complexes with FLAGELLIN SENSING 2 (FLS2) and EF-TU RECEPTOR (EFR), which are the pattern recognition receptors for the bacterial pathogen-associated molecular patterns flagellin (or the derived epitope flg22) and EF-Tu (or the derived epitope elf18), respectively; thereby regulating anti-bacterial immunity[3–5]. BAK1 and SERK1 also serve as co-receptors for BRASSINOSTEROID INSENSITIVE 1 (BRI1), which perceives BRs to regulate plant growth and development[6–8]. However, the molecular mechanisms underlying BAK1 activation or functional specificity in diverse signaling pathways remain largely unknown[1].

Previous knowledge of BAK1 phosphorylation is largely restricted to *in vitro* studies that identified phosphosites affecting overall BAK1 kinase activity[9–13], thus providing limited information about dynamic regulatory events *in vivo*. The specific identification of *in vivo* BAK1 phosphosites during immune signaling is impeded by the impaired functionality of epitope-tagged BAK1 variants in immunity[14], which could otherwise facilitate enrichment prior to mass-spectrometry-based phosphosite identification[9]. Furthermore, the involvement of BAK1 in multiple signaling pathways[2] makes difficult the identification of pathway-specific phosphosites from a total BAK1 cellular pool.

To gain insights into the mechanisms of BAK1 activation during immune signaling, we enriched endogenous BAK1 in complex with green fluorescent protein (GFP)-tagged FLS2 or EFR upon ligand treatment (Extended Data Fig. 1a, b), and then used tandem mass spectrometry to identify phosphosites of native, immune-active BAK1. To reduce residual levels of BR-activated BAK1, we pre-treated tissues with the BR biosynthesis inhibitor brassinazole (BRZ). This analysis identified four previously uncharacterized *in vivo* BAK1

phosphosites (S602, T603, S604 and S612; where T is Threonine, and S is Serine) (Extended Data Fig. 1c and Supplementary Figure 2 for spectra), in addition to T446 whose phosphorylation was previously shown to be dispensable for both BR and flg22 signaling[9]. Notably, S604 and S612 were previously identified as *in vitro* phosphosites[10].

To test functionality of these novel *in vivo* phosphosites, we generated stable transgenic Arabidopsis lines expressing non-phosphorylatable variants for these residues [substituting S/T with Alanine (A)] in the null *bak1–4* mutant[3] background and tested for functional complementation by measuring flg22-induced production of reactive oxygen species (ROS) as an early immune output[15]. In the case of the S602/T603/S604 sites, we utilized triple A mutants (hereafter AAA), as single or double mutations did not impair *bak1–4* complementation in mesophyll protoplasts (Extended Data Fig. 2a,b) or stable lines (Extended Data Fig 2c,d). Both the AAA and S612A mutants failed to complement flg22-induced ROS production in *bak1–4* (Fig. 1a, Extended Data Fig 3a,b). In contrast, corresponding phosphomimetic (S602D/T603D/S604D or S612D) mutants partially complemented the impaired ROS phenotype of *bak1–4* protoplasts, in keeping with the importance of these residues as phopshosites, although these mutations were not gain-of-function (Extended Data Fig 2e,f). Loss of S602/T603/S604 and S612 phosphorylation also impaired both flg22-induced MAP kinase (particularly MPK4/11) activation (Fig. 1b) and immunity to the bacterial pathogen *Pseudomonas syringae* pv. *tomato* (*Pto*) DC3000, resembling the semi-dominant mutant *bak1–5* (ref. 16) (Fig. 1c). This impaired immune function was not caused by impaired BAK1 accumulation or FLS2-BAK1 association (Fig. 1b, Extended Data Fig. 3c,d).

Critically, *bak1–4*/AAA and *bak1–4*/S612A lines were not impaired in their response to endogenous BR (Extended Data Fig. 4) or exogenously applied brassinolide (BL; the most biologically-active BR) or BRZ (Fig. 1d-f, Extended Data Fig. 4e). This demonstrates that the conserved S602/T603/S604 and S612 phosphosites[17] (Extended Data Fig. 5a, b) are required for flg22-induced immune responses, but are dispensable for BR signaling, and provides a mechanistic explanation for the phenotype caused by the deletion of the BAK1 C-terminal tail[18]. Using a phospho-specific antibody for S612 (Extended Data Fig. 5c, d), we observed that S612 phosphorylation is lost on C-terminally-tagged BAK1 variants (Extended Data Fig. 5e), which may underlie their previously documented non-functionality in immune signaling, although we cannot exclude the possibility of additional mechanism(s).

Plant RKs have emerged as dual-specificity kinases – similar to animal receptor tyrosine kinases[19] however, unbiased proteomics-based identification of phosphotyrosines in plant RKs is not trivial[20–21]. We therefore also individually mutagenized Tyrosine (Y) residues in the BAK1 cytoplasmic domain to non-phosphorylatable Phenylalanine (F), and tested for complementation of elf18-induced ROS in *bak1–4* mesophyll protoplasts. Y403F and Y463F mutations did not support ROS production, while Y365F was partially impaired (Extended Data Fig. 6a). The results with Y463F are consistent with previous findings that this residue is essential for BAK1 kinase activity[13], and thus we did not pursue its characterization. Considering, however, the strong impact of the Y403F mutation on elf18-induced ROS (Extended Data Fig. 6a), we generated *bak1–4*/Y403F lines (Extended Data Fig. 7a, c). BAK1-Y403F accumulated to wild-type levels and still formed a flg22-induced

complex with FLS2 (Extended Data Fig. 7a, b), but had an abrogated function in immunity (Fig. 2a-c). As with the AAA and S612A mutants (Fig. 1d-f; Extended Data Fig. 4), the Y403F mutation did not impair BR signaling (Fig. 2d-f; Extended Data Fig. 4e, 7c-e). Unlike phosphoserine/phosphothreonine, acidic residues are generally unable to mimic the charge and size of phosphotyrosine, consistent with the inability of Y403D to complement the elf18-induced ROS burst in *bak1–4* protoplasts (Extended Data Fig 6b,c).

The semi-dominant *bak1–5* mutation affects immune but not BR signaling in a similar manner to Y403F, and the causative mutation (C408Y) is near Y403 in the BAK1 catalytic loop[20] (Extended Data Fig. 8a). *In silico* substitution suggested C408Y creates steric hindrance with Y403 (Fig. 3a), which could affect its phosphorylation. To test this hypothesis, we generated C408Y, C408A, C408S or C408F BAK1 mutants, and assayed them for *bak1–4* complementation (Fig. 3a, b). Notably, only substitution with aromatic residues (C408Y and C408F) abolished BAK1 functionality (Fig. 3b), suggesting that the *bak1–5* phenotype is not caused by the creation of a new potential phosphosite (*i.e.* C408Y) or by loss of potential redox regulation on C408 (*e.g.* C408A, C408S)[23]. Using a phospho-specific pY403 antibody (Extended Data Fig. 9a,b), we determined that the C408Y and C408F mutations reduce Y403 phosphorylation *in vitro* (Fig. 3c), suggesting that the *bak1–5* phenotype is due to reduced Y403 phosphorylation, although we cannot fully exclude the possibility that additional mechanisms are also affected. Together with the finding that the Y403F mutation affects elf18-induced EFR complex phosphorylation (Fig. 3d,e)[21], these data suggest that Y403 phosphorylation is critical for the activation of immune signaling.

All BAK1 phosphosite mutants maintained both auto-phosphorylation (Extended Data Fig 9c,d) and substrate *trans*-phosphorylation (Extended Data Fig 9e) activities *in vitro*, though activity level varied between mutants (Extended Data Fig 9c-e). While loss of BAK1 activity causes defects in BR signaling[9], these mutants displayed no quantitative defects in BR signaling (Figure 1d-f, 2d-f). Phosphorylation on these sites is thus specifically associated with immune signaling and not solely BAK1 capacity as a kinase *per se*. Y403 and S612 are BAK1 auto-phosphorylation sites *in vitro* (Extended Data Fig. 9a,b), and, in the case of S612, auto-phosphorylation can occur in *trans* (Extended Data Fig 9f).

Altogether, our data could suggest a phosphosite-dependent uncoupling of BAK1 function between immunity and growth. However, upon close examination of Arabidopsis LRR-RK sequences, we noted that Y403 is strictly conserved in SERKs across plant species (Extended Data Fig. 8b), and that the analogous residue (which we refer to as Tyr-VIa, as it is present in kinase sub-domain VIa) is conserved in ~80% of Arabidopsis LRR-RKs regardless of their function in growth or immunity (Fig. 4a; Extended Data Fig. 10a; Supplementary Table 1). Notably, Tyr-VIa (Y836) phosphorylation is essential for EFR functionality, and Tyr RK phosphorylation is actively inhibited by bacteria to cause disease[21].

We thus postulated that functionality of LRR-RKs (acting as main ligand-binding receptors in diverse pathways) containing this conserved Tyr-VIa residue would require phosphorylation of this residue as well as of the analogous residue in their BAK1/SERK co-receptor(s). This hypothesis is so far supported by the fact that FLS2, EFR, PEP

RECEPTOR 1 and 2 (PEPR1/2) (which are immune receptors), as well as ERECTA (ER) and HAESA/HAESA-LIKE 2 (HAE/HSL2) (which are involved in development) are *bak1–5*-sensitive[5,16,24,25]. In contrast, the Tyr-VIa position in BRI1 is occupied by a Phe (Extended Data Fig. 10b), and BR signaling is not affected by either *bak1–5* (ref. 16) or BAK1-Y403F mutations (Fig. 2d-f; Extended Data Fig. 7c-e). We also show PEPR1/2 functionality requires BAK1-Y403 phosphorylation (Fig. 4b), and that phytosulfokine (PSK)-induced cell expansion mediated by PSK RECEPTOR 1 and 2 (PSKR1/2)[26] is also *bak1–5*- and BAK1-Y403F-sensitive (Fig. 4c). ER functionality also requires phosphorylation of its Tyr-VIa residue, as ER-Y760F is unable to complement the increased stomatal-lineage divisions or reduced pedicel length phenotypes of the *er-105* mutant[27] (Fig. 4d, e).

Altogether, our study suggests a phosphocode-based regulation that is most likely important for the functionality of the majority of Arabidopsis LRR-RKs. This work reveals a mechanism by which the common co-receptor BAK1 (and by extension related SERKs) differentially regulate at least two classes of ligand-binding LRR-RKs, named here as the Tyr-VIa-type and non-Tyr-VIa-type (Fig. 4a; Extended Data Fig. 10a, b; Supplementary Table 1). Interestingly, Arabidopsis CHITIN ELICITOR RECEPTOR KINASE 1 (CERK1) is a co-receptor for LysM-type RKs and also relies on phosphorylation of a Tyr-VIa residue[28]. Using structural modeling and sequence comparisons, we observed that an analogous Tyr-VIa residue is also conserved and phosphorylated in EPIDERMAL GROWTH FACTOR RECEPTOR (EGFR)[29], and is similarly conserved in several other animal tyrosine kinases (Extended Data Fig. 10c, d), which suggests that the Tyr-based regulation we have uncovered is important for different classes of RKs across kingdoms. Future structural work will be key to understand the molecular basis of this regulation.

Methods

Plant material and growth conditions

All plants used in this study were in the *Arabidopsis thaliana* accession Col-0 background. The following mutants were previously reported: *bak1–4*[3], *bak1–5*, *bri1–301 bak1–4*[16], *bak1–4*/pBAK1:BAK1[30], *bak1–4 bkk1–1*/pBAK1:BAK1-flag, *bak1–4*/pBAK1:BAK1-HA3, *bak1–4*/pBAK1:BAK1-eGFP[14], Col-0/pFLS2:FLS2-GFP[31], *efr-1*/pEFR:EFR-GFP[32], *er-105*[27] and *er-105*/pER:ER-YFP[3]. The ER-Y760F-YFP construct was introduced to the *er-105* background via Agrobacterium-mediated transformation using the floral dip method [34]. BAK1 WT and BAK1 phosphomutant constructs were similarly inserted to the *bak1–4* and *bri1–301 bak1–4* backgrounds via Agrobacterium-mediated transformation. Plants were grown on soil as one plant per pot in controlled rooms maintained at 20°C–22°C with a 10 h photoperiod or *in vitro* in Murashige and Skoog (MS) media supplemented with vitamins and 1% sucrose (Duchefa) with a 16 h photoperiod (at 22°C). Physiological assays were performed at 4–5 weeks on soil-grown plants or at 14 days post germination on *in vitro*-grown plants, unless differently specified. The *bak1–4*/*efr-1*/pEFR:EFR-GFP and lines were generated by genetic crossing. The *bak1–4/efr-1*/pEFR:EFR-GFP line was further crossed to *bak1–4*/pBAK1:BAK1 or *bak1–4*/pBAK1:BAK1-Y403F lines to generate the F1 individuals used in IP-kinase assays.

Molecular cloning

The coding sequence of BAK1 was inserted via BsaI digestion and ligation to the Golden Gate compatible vector pICSL22001 (generated by TSL Synthetic Biology group) for expression in protoplasts under the 35S promoter. The BAK1 single and multiple mutants were initially generated by BsaI digestion and ligation of respective PCR fragments to the pICSL22001 vector. The BAK1 phosphorylation mutants were PCR amplified from equivalent pICSL22001 plasmids and inserted using In-Fusion cloning (Clontech Laboratories) between BsrgI and BamHI restriction sites to an epiGreenB2 vector containing the whole genomic region of BAK1, with a 1445 bp promoter fragment [16,30]. Resulting constructs were transformed into *Agrobacterium tumefaciens* strain Agl1 containing the pSOUP helper plasmid. PCR-amplified fragments of cytoplasmic domain of BAK1 (BAK1-CD, aa 255–615) [35] and phosphorylation mutants were introduced into pOPINM vector (N-terminal 6xHis-MBP fusion) using In-Fusion enzyme (Clontech Laboratories) for recombinant protein expression. The GST-BAK1 and GST-BAK1–5 are in the pGEX-4T1 vector and were previously described [16]. The kinase dead (D416N) in the pOPINM vector and C408F mutation in the pGEX-4T1 vector (N-terminal GST fusion) were generated using a DpnI-mediated site-directed mutagenesis protocol. The D416N mutation was also introduced into a pET28a (+):BAK1-CD (aa 250–615) clone that was kindly provided by Kyle W. Bender and Raymond Zielinski (University of Illinois) using DpnI-mediated mutagenesis. The GST-BIK1* (K105E) clone in pGEX-4T1 was previously described[36]. To express ER Y760F in plants, pJM284 (pER:ER-YFP) [33] was used as a template for site-directed mutagenesis and was further transformed into the *Agrobacterium tumefaciens* strain GV3101/pMP90. Sequences of all primers used in this study are listed in Supplementary Table 2.

Chemicals

Synthetic flg22, elf18, and AtPep1 peptides were purchased from EZBiolab. Peptide sequences for flg22, elf18, and AtPep1 have been previously described [36–38]. Synthetic PSK-α peptide [26] was purchased from PeptaNova GmbH. All peptides were dissolved in sterile water. EpiBL was purchased from Xiamen Topusing Chemical and prepared as 20 mM stock solution in ethanol. Brassinazole (BRZ) was purchased from Sigma and prepared as 10 mM stock solution in DMSO.

Immunity-related bioassays

ROS burst and MAPK activation and bacteria spay infections were performed as previously described [30,39].

Protoplast assays

Arabidopsis mesophyll protoplasts isolation and transfections were performed as previously described [40] and the protocol was further optimized to measure ROS burst. Briefly, following the plasmid transfection and washing step, the protoplasts are resuspended in a W5 buffer containing 154 mM NaCl, 125 mM $CaCl_2$, 5 mM KCl, and 2 mM MES adjusted with 2 mM Tris to pH 8, and directly distributed to a 96-well plate (100 μL of protoplast suspension per well). The protoplasts were left to rest for 16 h prior to treatment. Protoplasts

were gently treated with luminol L-O12 (Wako Chemicals) (4 μM final concentration), HRP (10 μg/mL final concentration) and the indicated elicitor peptide in the same W5 pH 8.0 solution (final volume 200 μl/well). In the case of flg22-induced ROS, protoplasts were co-transfected with a 35S:FLS2-FLAG construct [41]. Luminescence was recorded over a 40–60 min period using a charge-coupled device camera (Photek Ltd., East Sussex UK).

For PSK-induced protoplast swelling assays Arabidopsis mesophyll protoplasts were isolated by digestion of cell walls as described previously [40], resuspended in a W5 buffer containing 2 mM MES 5.7, 154 mM NaCl, 125 mM CaCl2, 10 mM KCl [26,42] and kept in the dark prior to treatment. Protoplasts were then treated with 1 nM PSK-α solution and observed under 10x magnification on a Leica DMB5500B fluorescent microscope. Images were acquired every 5 min over a period of 30 min. ImageJ software was used to measure the circumference of the protoplasts from which the net volume change was calculated.

BR-sensitivity assay

Seeds were surface sterilized and individually placed in line on square petri dishes containing ½ MS, 1% sucrose, 0.8% phytoagar and 2 μM of BRZ. The plates were placed in the cold for 2 days and then placed vertically in a growth chamber for 6 d. Then pictures of the plates were taken to measure root lengths were measured using the ImageJ software. For root growth inhibition assay 5 nM of BL were added to a similar media containing 0.5 μM BRZ. For hypocotyl growth in the dark assay, plates were moved from cold to light for 3 h to stimulate germination, before wrapping them in tin foil and then placing them vertically in the growth room for 6 days. For BES1 dephosphorylation assays, seedlings were germinated on MS-agar supplemented with 1% sucrose for 5 d before transplanting to 6-well plates (5 seedlings/well). One day prior to assays, seedlings were treated with 2 μM BRZ (final concentration). Twelve-day-old seedlings were treated with BL or ethanol (mock) at concentrations indicated for 60 min.

Western blot

Western blot analysis was performed with antibodies diluted in blocking solution (5% nonfat milk in TBS with 0.1% [v/v] Tween) at the following dilutions: α-GFP-HRP (B-2, Santa Cruz), 1:5000; α-MBP-HRP (NEB), 1:5000; α-p44/42-ERK (Cell Signaling Technology), 1:3000; α-FLS2, 1:1000[4]; α-BAK1, 1:5000 [5]. The polyclonal α-pY403 and α-pS612 antibodies were produced by Abmart and raised against ARGLA(pY)LHDHC and C-QIENEYP(pS)GPR epitope peptides respectively and were used in 1:1000 dilution. The α-BES1 antibodies were produced by GenScript against the (C)EDLELTLGNGKAHS epitope peptide and were kindly provided as a gift from Prof. Steven Huber (University of Illinois), and were used in 1:1000 dilution. In the case of immunoblotting of *in vitro* samples, blots were blocked with TBS with 0.1% (v/v) Tween, 5% gelatin from cold water fish skin (Sigma), and probed with the following antibodies in the same blocking solution: α-pTyr-HRP (PY99, Santa Cruz), 1:2000; α-pThr (P-Thr-Polyclonal, Cell Signaling), 1:1000; α-BAK1, 1:5000; α-pY403, 1:1000; α-pS612, 1:3000. The following secondary antibodies were used: α–Rabbit IgG-HRP Trueblot (Rockland, 18–8816-31, dilution 1:10000) for detection of BAK1-FLS2 co-IPs or α-rabbit IgG (whole molecule)–HRP (A0545, Sigma, dilution 1:10000) for all other western blots.

Immunoprecipitation and protein purification

FLS2-BAK1 IPs were performed as previously described [14]. EFR-GFP IPs coupled with kinase assays were performed as previously described [21]. Large scale EFR-GFP and FLS2-GFP IPs were performed for *in vivo* discovery of BAK1 phosphorylation sites. Arabidopsis Col-0/pFLS2:FLS2-GFP and *efr-1*/pEFR:EFR-GFP seedlings were grown in MS medium, 1% sucrose (plus vitamins) (Duchefa) in 6-well plates (5 seedlings per well) for two weeks. One day prior treatment, 100 nM BRZ (final) was added to the media. About 30 g of tissue per condition was treated with 1 μM elf18, flg22 or MS alone as mock control for 10 min (including 4 min of vacuum infiltration) and frozen in liquid nitrogen. Tissue was ground with liquid nitrogen to a fine powder and resuspended in 2 mL/g powder of extraction buffer [150 mM Tris-HCl, pH 7.5; 150 mM NaCl; 5mM EDTA; 1% Igepal; 1% (vol/vol) protease inhibitor mixture, phosphatase inhibitor 2 and 3 (Sigma), 1mM Na_3VO_4]. Immunoprecipitation was performed with GFP-Trap beads, as previously done [21]. Immunoprecipitates were eluted in SDS loading buffer and proteins were further analyzed by SDS-PAGE and Western blot.

6xHis-MBP- or GST-tagged proteins were purified by Ni^{2+} affinity chromatography using Ni Sepharose High Performance (GE Healthcare) or GST-Bind (Millipore) resin, respectively. Following elution, proteins were immediately concentrated and washed using Amicon® Ultra-4 Centrifugal Filter Concentrators (MWCO 4000, Millipore) and stored in buffer (25 mM Tris-Cl, 10% glycerol, 1 mM DTT, pH 7.5) until use in assays. For gel and blot source data, see Supplementary Figure 1.

Kinase assays

Unlabeled *in vitro* kinase assays were performed as previously described [35] with the difference that 10 μM unlabeled ATP was used and specific phosphorylation was detected with the phospho-specific antibodies as described in figure captions. To detect autophosphorylation *in trans*, assays were performed the same but with 100 μM unlabeled ATP for 60 min. *In vitro* kinase assays with labeled [^{32}P]γ-ATP and EFR-GFP immunoprecipitation-coupled kinase assays were performed as previously described [21]. Quantification of ^{32}P autoradiography bands was performed using the ImageJ software. For gel and blot source data, see Supplementary Figure 1.

Mass spectrometry analysis

Proteins were separated by SDS-PAGE (NuPAGE, Invitrogen), and after staining with SimplyBlue stain (Invitrogen) bands corresponding to BAK1 were excised and digested by Trypsin and AspN. LC-MS/MS analysis was performed with a Orbitrap Fusion Trihybrid mass spectrometer (Thermo Scientific) and a nanoflow-HPLC system (Dionex Ultimate3000, Thermo Scientific) as described previously [43]. The peptide identification was performed by searching the Arabidopsis database (TAIR10) using Mascot (v 2.4.1 Matrix Science) as described previously [43] with the modification of allowing Trypsin and AspN peptide termini. Scaffold (v4; Proteome Software) was used to validate MS/MS-based peptide and protein identifications and annotate spectra. The position of the modified residue and the quality of spectra for individual phosphopeptides were manually inspected and validated.

Confocal microscopy

The epidermal phenotypes were observed using confocal microscopes, Zeiss LSM700 (for cell periphery stained with propidium iodide [ThermoFisher Scientific]) and Leica SP5-WLL (for YFP fluorescence) as described previously [44].

In silico analysis

Structural comparisons were performed using the DALI server [45]. The structure figures were prepared using PYMOL molecular viewer (http://www.pymol.org/). Arabidopsis LRR-RLKs were identified based on previous reports [46,47], and protein sequences corresponding to the representative gene model of each were downloaded from TAIR10. Cytoplasmic RKs (lacking a clear ectodomain) were removed, resulting in a final list of 229 LRR-RLKs, presented in Supplementary Table 1. These LRR-RKs were arranged by gene ID within previously assigned subgroups, and cytoplasmic domains were aligned by Clustal Omega to generate the WebLogos and alignments shown in Fig. 4a and Extended Data Fig. 9, respectively.

Statistical analysis

Stastistical analysis was performed using one-way ANOVA analysis of variance (ANOVA) test and Dunnett's post-test, as implemented in GraphPad Prism 7.0. (GraphPad Software, http://www.graphpad.com).
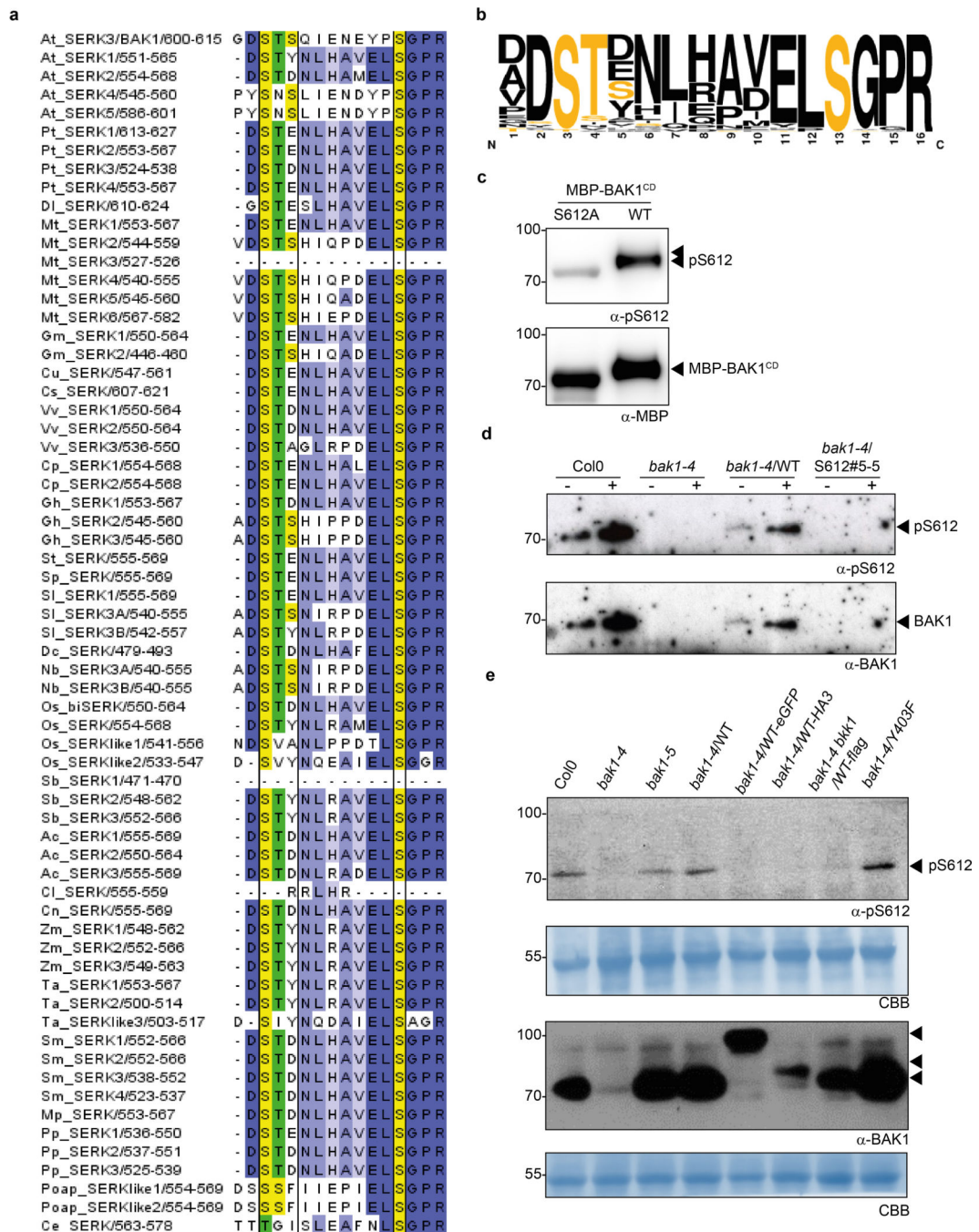
Extended Data

Figure 1 |. Identification of BAK1 phosphosites.

a, Representative Coomasie brilliant Blue (CBB)-stained SDS-PAGE gel showing proteins enriched upon GFP immune-precipitation. **b**, Western blot analysis of BAK1 co-immunoprecipitated with FLS2-GFP and EFR-GFP proteins from (**a**) using α-GFP and α-BAK1 antibodies. **a**, **b,** Experiments were independently repeated three times. For gel and blot source data, see Supplementary Figure 1. **c**, Summary of BAK1 *in vivo* phosphosites

identified by FLS2-GFP and EFR-GFP co-immunoprecipitation followed by LC-MS/MS analysis. Spectra of identified sites are presented in Supplementary Figure 2.
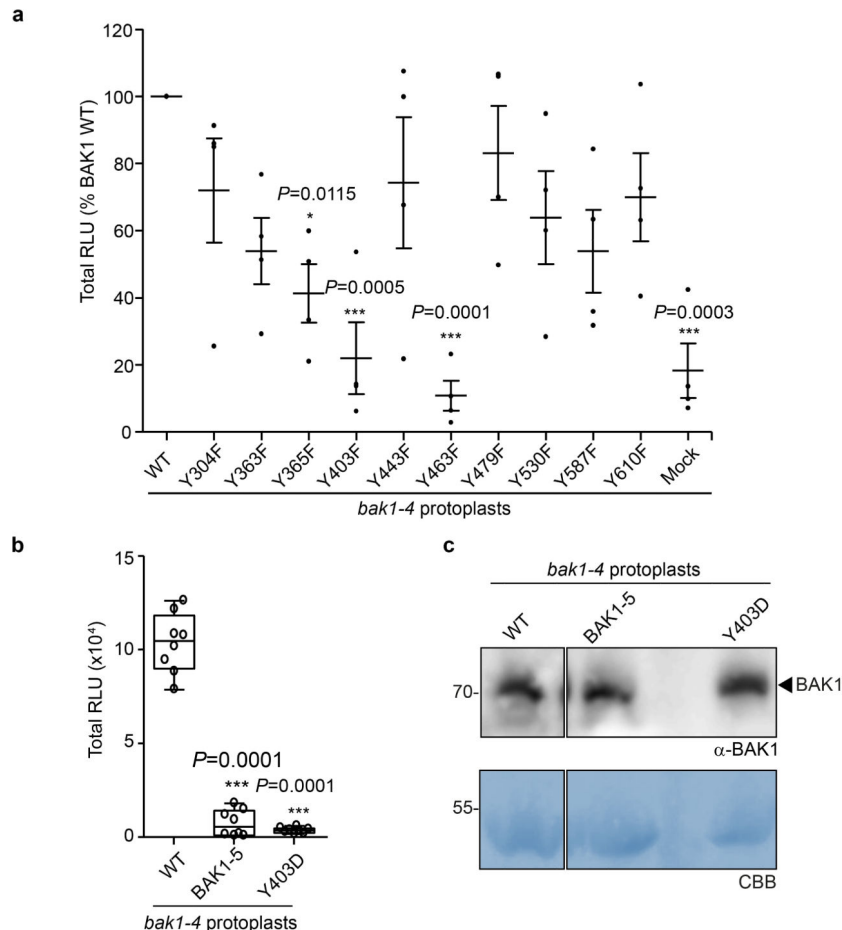

Figure 2 |. Individual or double BAK1-S602A, -T603A, or -S604A mutations do not affect elf18-induced ROS production.

a, e, Total ROS production following treatment with 100 nM elf18 over 60 min of n=12 biological independent suspensions of *bak1–4* mesophyll protoplasts transiently expressing the indicated BAK1 mutants,. **b, d, f,** Western blot analysis with α-BAK1 antibodies. For blot source data, see Supplementary Figure 1. **c,** Total ROS production following treatment of n=8 biologically independent leaf discs with 100 nM flg22 over 40 min. Circles indicate individual data points. **a,c,e,** Measurements are plotted as boxplots displaying the first and third quartiles, split by the median; whiskers extend to a maximum of 1.5 × interquartile range beyond the box. Outliers are indicated as black dots. Statistical analysis was performed using one-way ANOVA and Dunnett's post-hoc test compared to WT BAK1. **a-e,** Experiments were repeated at least three times.
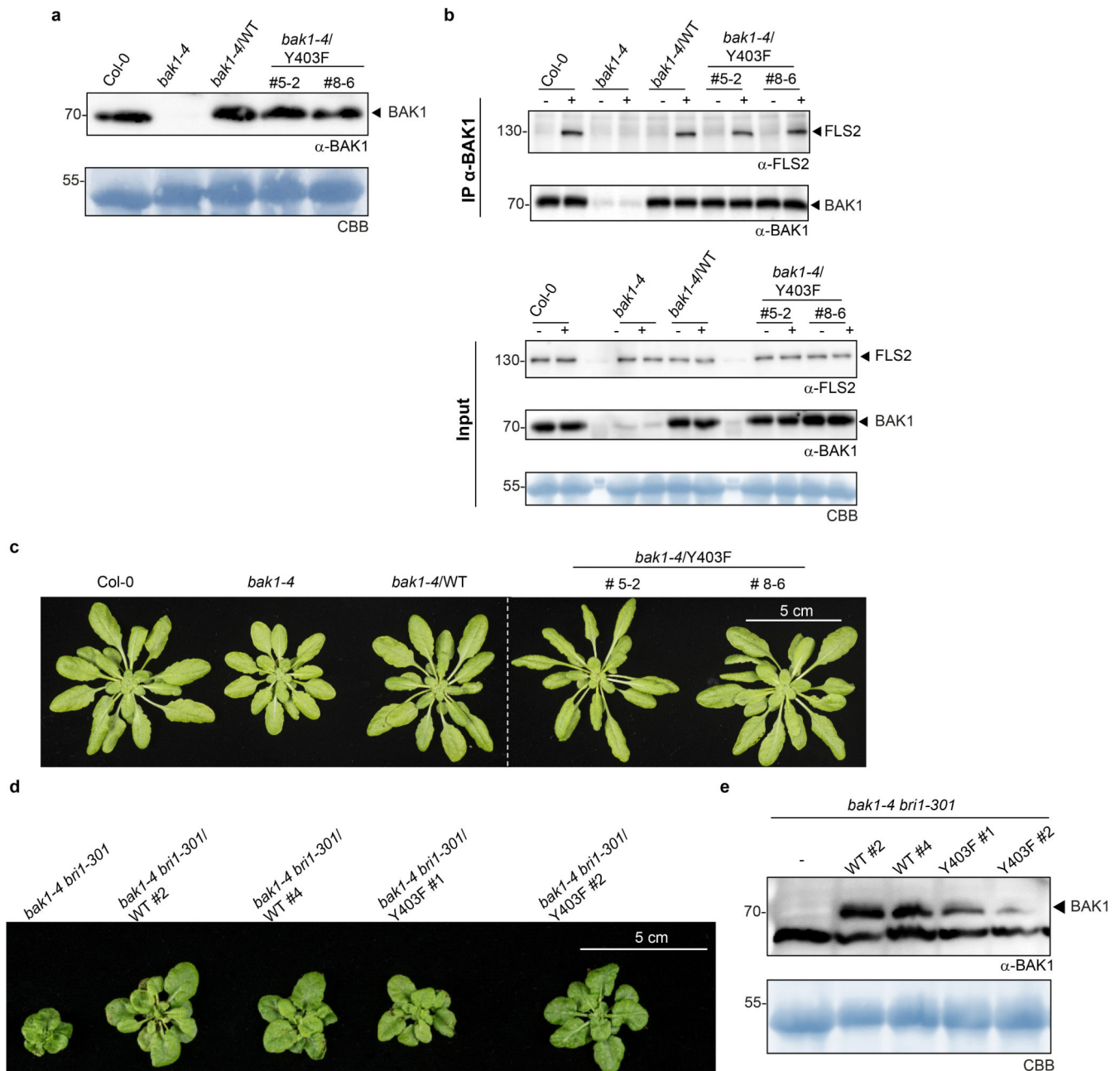
Figure 3 |. BAK1-AAA and BAK1-S612A plants are not affected in flg22-induced FLS2-BAK1 complex formation.

a, b, Western blot analysis with α-BAK1 antibodies. **c, d,** Co-immunoprecipitation between FLS2 and BAK1 using α-FLS2 and α-BAK1 antibodies. Two-week-old seedlings were treated with water (−) or 100 nM flg22 (+) for 10 min before protein extraction. Blots were stained with Coomassie brilliant blue (CBB) for loading control. **a-d,** Experiments were repeated at least three times with similar results. For blot source data, see Supplementary Figure 1.
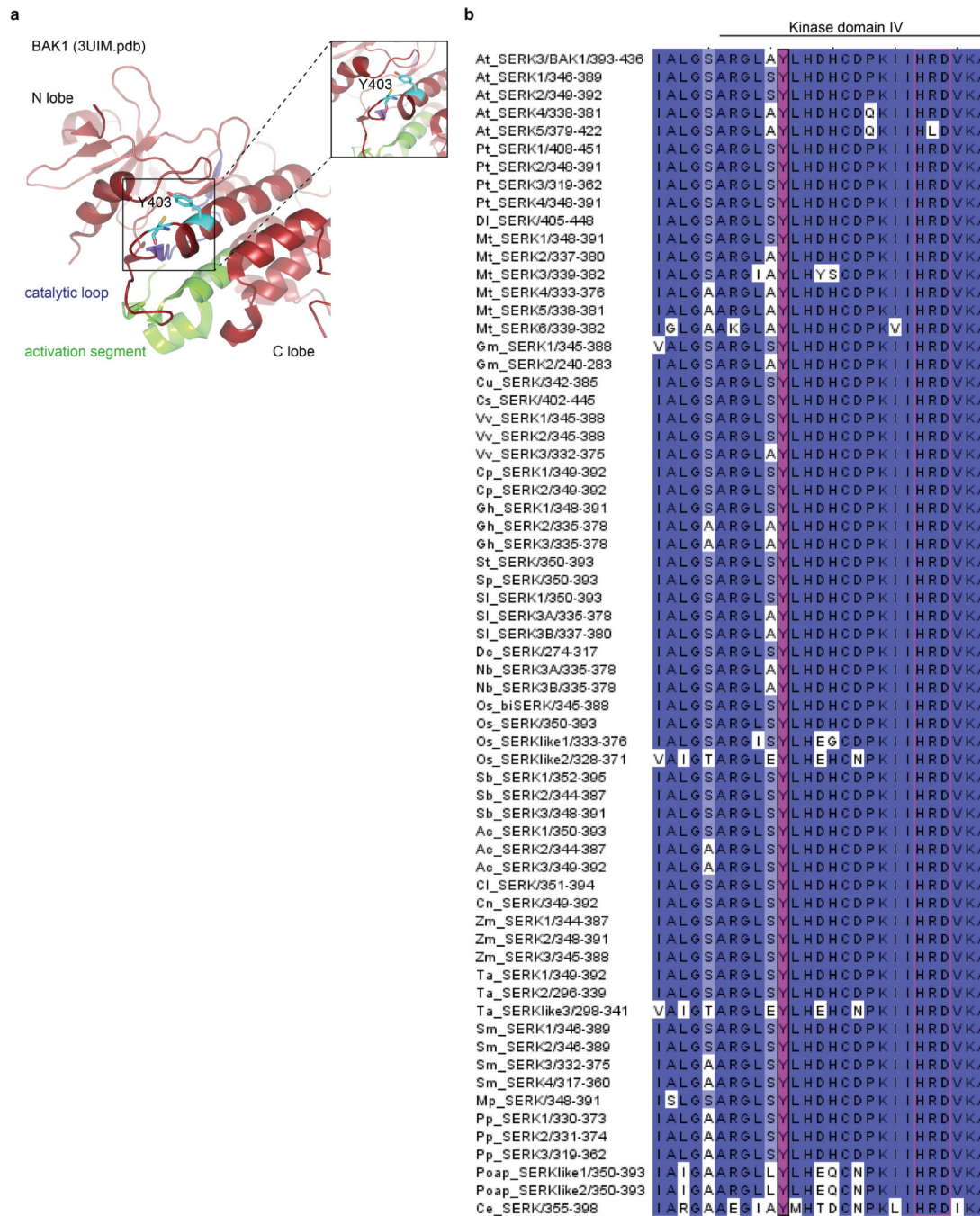
Figure 4 |. Expression of the BAK1-AAA and BAK1-S612A variants restores the semi-dwarf rosette phenotype of *bak1–4* and *bak1–4 bri1–301*

a, b, Representative images of rosettes from 4- to 5-week-old plants. **c, d,** Left, representative images of rosettes from 5- to 7-week-old plants. Right, western blot analysis with α-BAK1 antibodies. Blots were stained with Coomassie brilliant blue (CBB) for loading control. Experiments were repeated at least twice with similar results. Control plants used in (b), were previously pictured [30]. **e,** BES1 de-phosphorylation 60 min after treatment of 10-day-old seedlings with the indicated concentrations of epi-BL, as shown by western

blot analysis using α-BES1 antibodies. Blots were probed with α-BAK1 antibodies, and subsequently stained with Coomassie brilliant blue (CBB) as loading controls. **a-e,** Experiments were repeated at least three times. For blot source data, see Supplementary Figure 1.
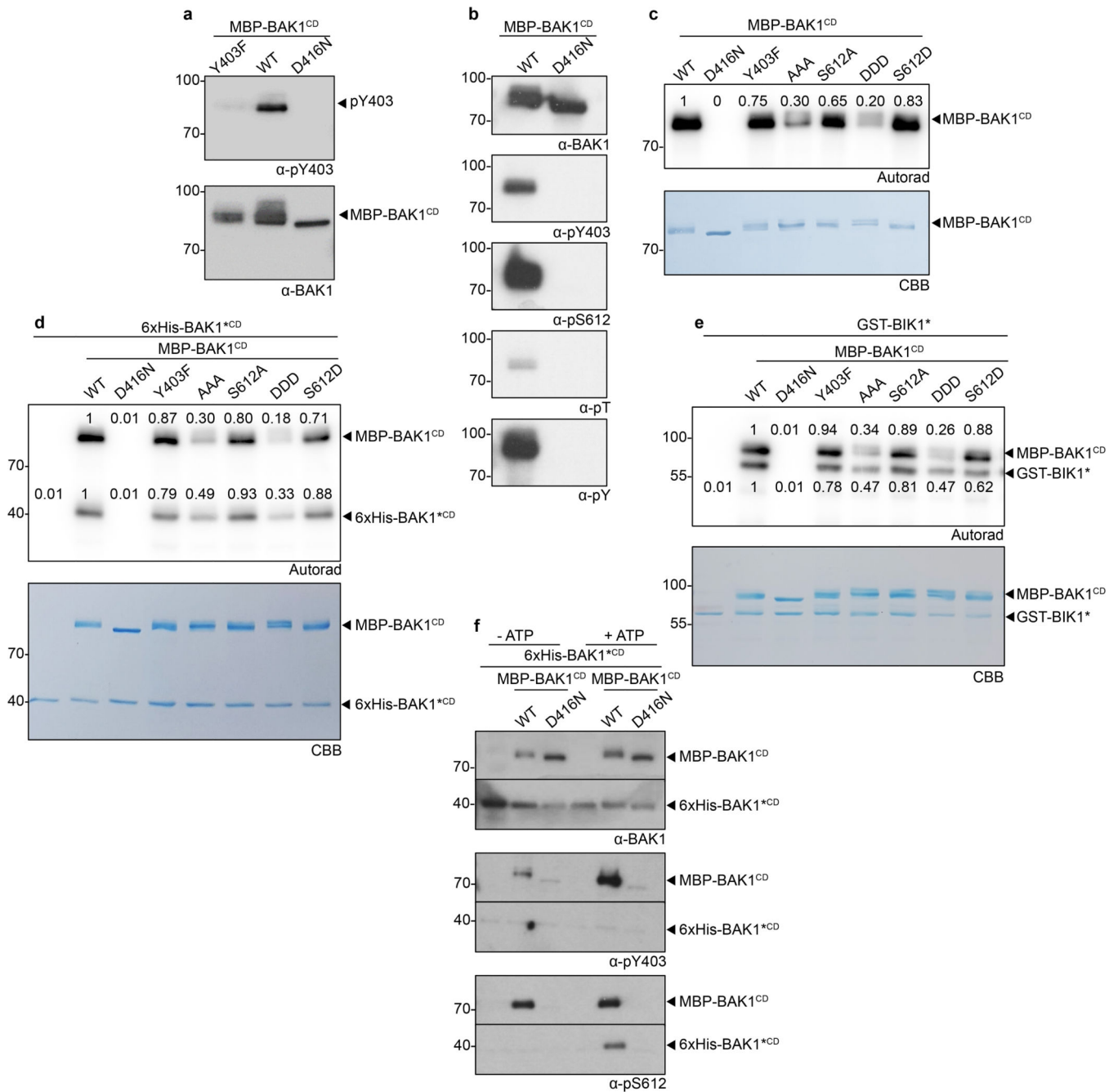

Figure 5 |. Conservation of BAK1 C-terminal tail phosphosites in SERK proteins across plant species.
a, Clustal Omega multiple alignments were visualized using JalView v2.10.2b2. The alignment is coloured by percentage identity. Yellow, conservation of BAK1-S602, -S604

and -S612; green, conservation of BAK1-T603. Protein IDs used for the alignments: PpSERK1(B9MW41), PpSERK2(B9IQM9), PpSERK3(B9HFX1), PpSERK4(B9H599),DlSERK(B5TTV0), MtSERK1(Q8GRK2), MtSERK2(E2IXG1), MtSERK3(E2IXG8), MtSERK4(E2IXG2), MtSERK5(E2IXG3), MtSERK6(E2IXG4), GmSERK1(C6ZGA8), GmSERK2(C6FF61), CuSERK (Q6BE26), CsSERK(C3V9W0), VvSERK1(D7TXV2), VvSERK2(A5BIY4), VvSERK3(D7STF6), CpSERK1(A7L5U3), CpSERK2(E5D6S9), GhSERK1(E5Q8K6), GhSERK2(F5BZU9), GhSERK3(F6MF11), StSERK(A3R789), SpSERK(A6N8J2), SlSERK1(G0XZA3), SlSERK3A(G0XZA5), SlSERK3B(G0XZA6), DcSERK(O23921), AtSERK1(Q94AG2), AtSERK2(Q9XIC7), AtSERK3(Q94F62), AtSERK4(Q9SKG5), AtSERK5(Q8LPS5), NbSERK3A(E3VXE6), NbSERK3B(E3VXE7), OsbiSERK(Q6S7F1), OsSERK(Q5Y8C8), OsSERKlike1(Q67X31), OsSERKlike2(Q6K4T4), SbSERK1(C5YHV3), SbSERK2(C5Y9S6), SbSERK3(C5XVP5), AcSERK1(H6SU43), AcSERK2(H6UP78), AcSERK3(H6UP79), ClSERK(G2XLB1), CnSERK(Q5S1N9), ZmSERK1(Q93W70), ZmSERK2(Q94IJ5), ZmSERK3(B4G007), TaSERK1(G4XGX1), TaSERK2(G4XGX2), TaSERKlike3(G4XGX3), SmSERK1(D8SBB8), SmSERK2(D8S0N3), SmSERK3(D8S4M4), SmSERK4(D8R6C9), MpSERK(A7VM18), PpSERK1(A9STU8), PpSERK2(A9SMW5), PpSERK3(A9RY79), PoapSERKlike1(Q659J0), PoapSERKlike2(Q659J1), CeSERK(A7VM46). **b,** WebLogo representation of alignment in **(a).**

c, Detection of BAK1-S612 phosphorylation using α-pS612 specific antibodies on affinity-purified recombinant BAK1^{CD} following an *in vitro* kinase assay with cold ATP. Membranes were immuno-blotted with α-pS612 and α-MBP antibodies. **d,** BAK1 immunoprecipitation (IP) and detection of BAK1-S612 phosphorylation *in vivo* using α-pS612 antibodies. Two-week-old seedlings were treated with water (−) or 100 nM flg22 (+) for 10 min. The same membrane was stripped and blotted again with α-BAK1 antibodies for loading control. **e,** Western blot analysis using α-BAK1 and α-pS612 antibodies after SDS-PAGE of crude protein extracts from two-week-old seedlings treated with 100 nM flg22 for 10 min. Blots were stained with Coomassie brilliant blue (CBB) for loading control. **a-e,** All experiments were repeated at least twice with similar results. For blot source data, see Supplementary Figure 1.

Figure 6 |. Mutational screen of Tyr residues present in BAK1 cytoplasmic domain.
a, Total ROS production following treatment of *bak1–4* mesophyll protoplasts with 100 nM
elf18 over 30 min. The total relative luminescence unit (RLU) values from n=4 independent
biological experiments are normalized relative to protoplasts expressing wild-type (WT)
BAK1 and expressed as aligned dot blots showing mean ± SE. **b,** Total ROS production
following treatment with 100 nM elf18 over 60 min of n=8 biologically independent
suspensions of *bak1–4* mesophyll protoplasts transiently expressing the indicated BAK1
mutants,. Measurements are plotted as boxplots displaying the first and third quartiles, split

by the median; whiskers extend to a maximum of $1.5 \times$ interquartile range beyond the box. Circles indicate individual data points. **c**, Western blot analysis with α-BAK1 antibodies. For blot source data, see Supplementary Figure 1. **a-b,** Statistical analysis was performed using one-way ANOVA and Dunnett's post-hoc test compared to the WT control. **b,c,** Experiments were repeated twice with similar results.
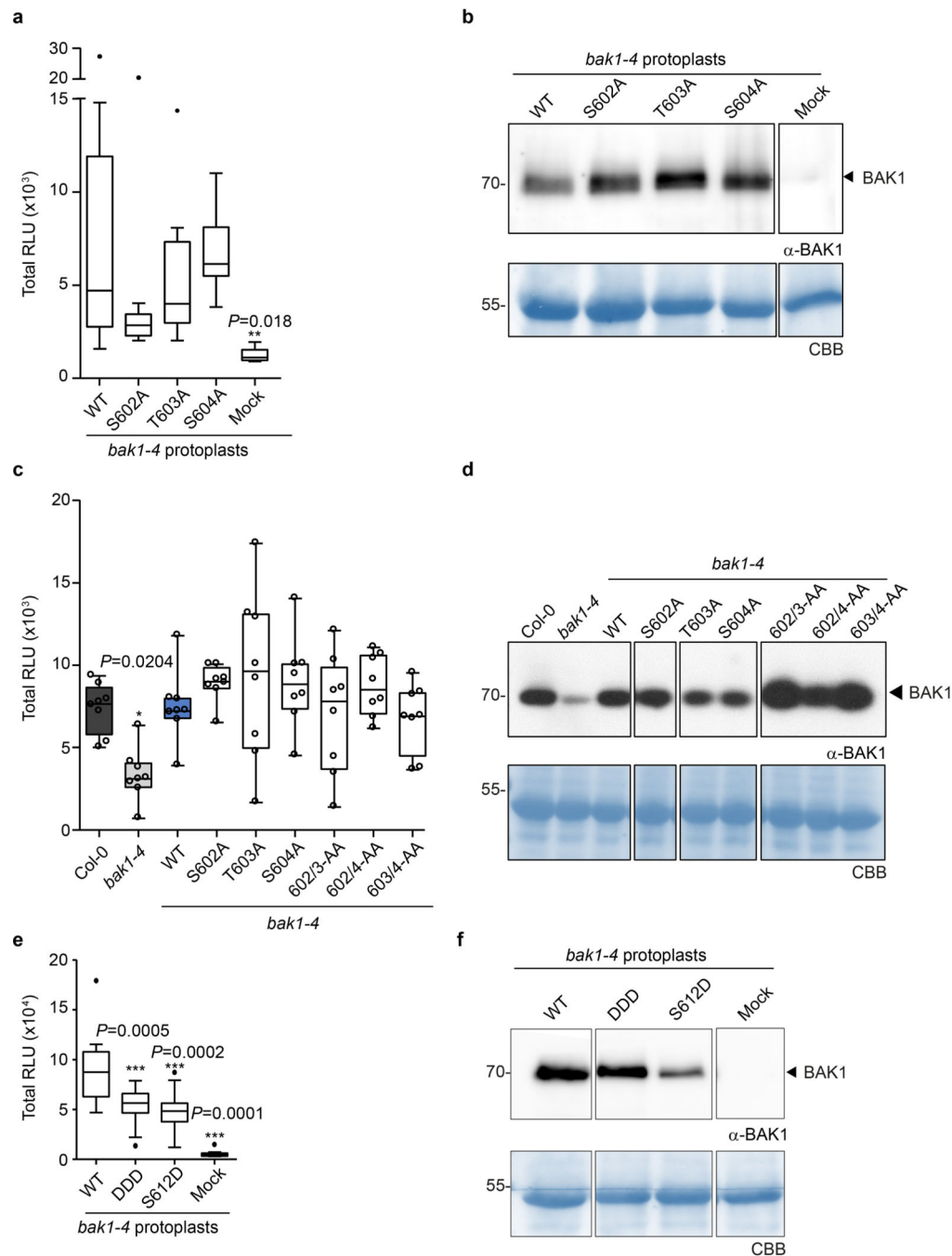

Figure 7 |. BAK1-Y403 plants are not affected in flg22-induced FLS2-BAK1 complex formation and brassinosteroid-mediated rosette growth.

a, Western blot with α-BAK1 antibodies. Blots were stained with Coomassie brilliant blue (CBB) for loading control. **b,** Co-immunoprecipitation between FLS2 and BAK1 using α-FLS2 and α-BAK1 antibodies. Two-week-old seedlings were treated with water (−) or 100 nM flg22 (+) for 10 min before protein extraction. Blots were stained with Coomassie brilliant blue (CBB) for loading control. **c,** Representative images of rosettes from 4- to 5-week-old plants. **d,** Representative images of rosettes from 5-week-old plants. Same control plants used in (d) were also presented in Extended Data Figure 4c. **e,** Western blot with α-BAK1 antibodies. Blots were stained with Coomassie brilliant blue (CBB) for loading control. **a-e,** Experiments were repeated three times with similar results. For blot source data, see Supplementary Figure 1.
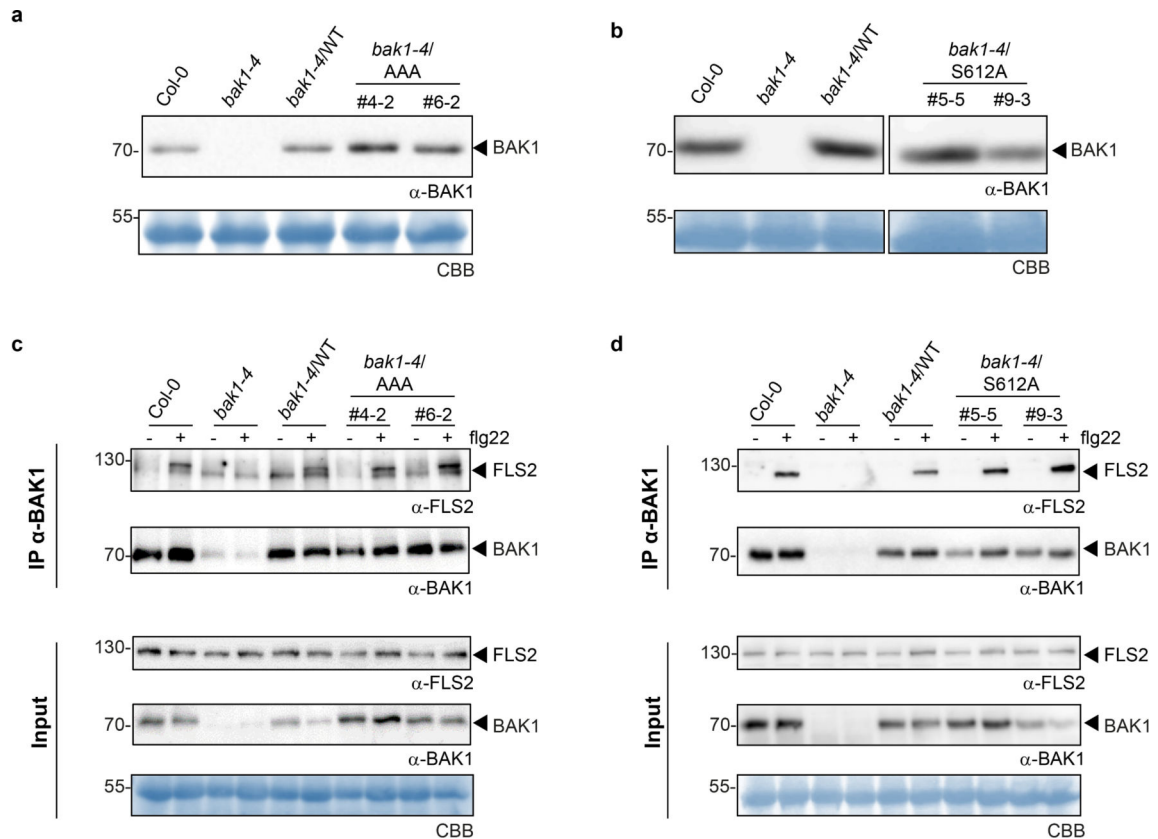

Figure 8 |. The conserved Tyr-VIa residue BAK1-Y403 is in close proximity to the catalytic loop and C408.

a, *In silico* representation of BAK1 cytoplasmic domain (BAK1^{CD}) structure (3UIM.pdb). The activation segment region is presented in green and the catalytic loop in purple. **b,** Conservation of BAK1-Y403 in SERK proteins across plant species. Clustal Omega multiple alignments were visualized using JalView v2.10.2b2. The alignment is coloured by percentage identity. Magenta, conservation of BAK1-Y403. Protein IDs used for the alignments: PpSERK1(B9MW41), PpSERK2(B9IQM9), PpSERK3(B9HFX1), PpSERK4(B9H599),DlSERK(B5TTV0), MtSERK1(Q8GRK2), MtSERK2(E2IXG1), MtSERK3(E2IXG8), MtSERK4(E2IXG2), MtSERK5(E2IXG3), MtSERK6(E2IXG4), GmSERK1(C6ZGA8), GmSERK2(C6FF61), CuSERK (Q6BE26), CsSERK(C3V9W0),

VvSERK1(D7TXV2), VvSERK2(A5BIY4), VvSERK3(D7STF6), CpSERK1(A7L5U3), CpSERK2(E5D6S9), GhSERK1(E5Q8K6), GhSERK2(F5BZU9), GhSERK3(F6MF11), StSERK(A3R789), SpSERK(A6N8J2), SlSERK1(G0XZA3), SlSERK3A(G0XZA5), SlSERK3B(G0XZA6), DcSERK(O23921), AtSERK1(Q94AG2), AtSERK2(Q9XIC7), AtSERK3(Q94F62), AtSERK4(Q9SKG5), AtSERK5(Q8LPS5), NbSERK3A(E3VXE6), NbSERK3B(E3VXE7), OsbiSERK(Q6S7F1), OsSERK(Q5Y8C8), OsSERKlike1(Q67X31), OsSERKlike2(Q6K4T4), SbSERK1(C5YHV3), SbSERK2(C5Y9S6), SbSERK3(C5XVP5), AcSERK1(H6SU43), AcSERK2(H6UP78), AcSERK3(H6UP79), ClSERK(G2XLB1), CnSERK(Q5S1N9), ZmSERK1(Q93W70), ZmSERK2(Q94IJ5), ZmSERK3(B4G007), TaSERK1(G4XGX1), TaSERK2(G4XGX2), TaSERKlike3(G4XGX3), SmSERK1(D8SBB8), SmSERK2(D8S0N3), SmSERK3(D8S4M4), SmSERK4(D8R6C9), MpSERK(A7VM18), PpSERK1(A9STU8), PpSERK2(A9SMW5), PpSERK3(A9RY79), PoapSERKlike1(Q659J0), PoapSERKlike2(Q659J1), CeSERK(A7VM46).
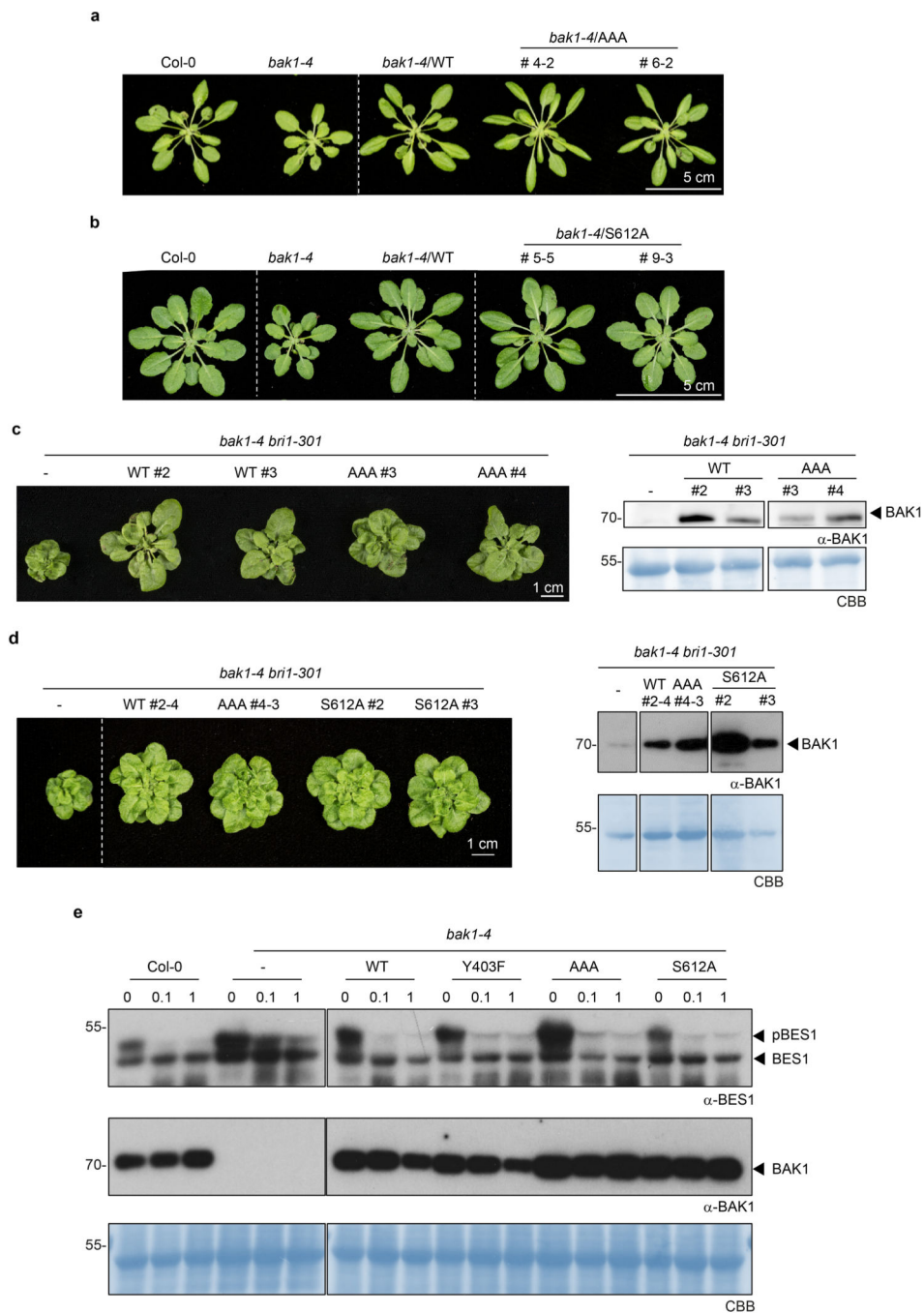
Figure 9 |. Analysis of phosphosite-specific kinase activities of BAK1

a, Specific detection of BAK1-Y403 phosphorylation on affinity-purified recombinant BAK1^{CD} WT but not Y403F or kinase-dead (D416N) proteins, using α-pY403 antibodies and following an *in vitro* kinase assay with cold ATP. Blots were probed with α -BAK1 antibodies for loading control. **b**, Detection of BAK1-Y403, -S612, -threonine (T) and - tyrosine (Y) phosphorylation using phosphorylation specific antibodies on affinity-purified recombinant BAK1^{CD} following an *in vitro* kinase assay with cold ATP. Membranes were immuno-blotted with BAK1 antibodies for loading control. **c**, Trans-autophosphorylation of

kinase-dead (D416N) BAK1 substrate (6xHis-BAK1*CD) at S612 by BAK1-WT (MBP-BAK1CD). BAK1-Y403 or-S612 phosphorylation was detected using phosphorylation specific antibodies following an *in vitro* incubation of the purified proteins in the presence or absence of cold ATP. Membranes were immuno-blotted with BAK1 antibodies for loading control. **d,** [32P] γ-ATP kinase assay showing autophosphorylation of the indicated affinity purified recombinant BAK1CD mutants. **e,** [32P] γ-ATP kinase assay showing trans auto-phosphorylation of the kinase-dead BAK1-D416N (6xHis-BAK1*CD) by wild type BAK1 (MBP-BAK1CD). **f,** [32P]γ-ATP kinase assay showing transphosphorylation activity of the indicated affinity purified recombinant BAK1CD mutants against a kinase-dead (K105E) BIK1 substrate (GST-BIK1*). Numbers indicate autoradiograph band intensity relative to WT. Protein loading control was determined with Coomasie brilliant blue (CBB) staining. **a-f,** All experiments were repeated independently at least three times. For blot source data, see Supplementary Figure 1.

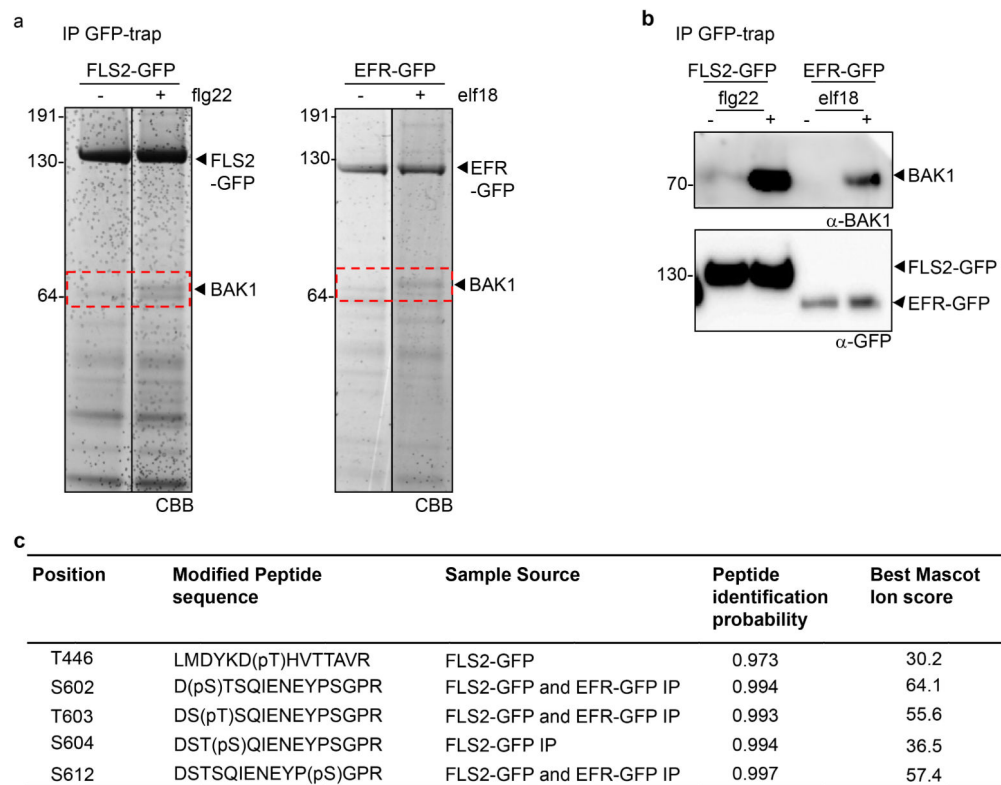| Position	Modified Peptide sequence	Sample Source	Peptide identification probability	Best Mascot Ion score
T446	LMDYKD(pT)HVTTAVR	FLS2-GFP	0.973	30.2
S602	D(pS)TSQIENEYPSGPR	FLS2-GFP and EFR-GFP IP	0.994	64.1
T603	DS(pT)SQIENEYPSGPR	FLS2-GFP and EFR-GFP IP	0.993	55.6
S604	DST(pS)QIENEYPSGPR	FLS2-GFP IP	0.994	36.5
S612	DSTSQIENEYP(pS)GPR	FLS2-GFP and EFR-GFP IP	0.997	57.4

Figure 10 |. Multiple alignment of *Arabidopsis thaliana* LRR-RK cytoplasmic domain illustrating the conservation (a) or non-conservation (b) of Tyr-VIa, and conservation of Tyr-VIa in representative members of the 20 groups of animal receptor tyrosine kinases.
a, b, Clustal Omega multiple alignments were visualized using JalView v2.10.2b2. The alignment is coloured by percentage identity. Magenta, Tyr-VIa. Protein IDs for the sequences used for the alignment are in Supplementary Table 1. Arrows indicate the LRR-RKs reported in this study. **c,** *In silico* alignments of BAK1CD and EGFRCD structures. A selected overlapping region of the BAK1 (3UIM.pdb) and EGFR (2JIT.pdb) cytoplasmic domain structures is presented, highlighting BAK1-Y403 and EGFR-Y827. **d,** Clustal Omega multiple alignments were visualized using JalView v2.10.2b2. The alignment is

coloured by percentage identity. Red, position analogous to BAK1-Y403. Protein IDs used for the alignments: EGFR (P00533), AXL (P30530), DDR15 (Q08345), EphA1 (P21709), FGFR2 (P21802), HGFR (P08581), INSR (P06213), PTK7 (Q13308), LTK (P29376), MUSK (O15146), PGFRB (P09619), RET (P07949), RYK (P34925), TIE1 (P35590), NTRK1 (P04629), VGFR1 (P17948), ROR1 (Q01973), ROS (P08922), LMR1 (Q6ZMQ8), STYK (Q6J9G0).

Supplementary Material

Refer to Web version on PubMed Central for supplementary material.

Acknowledgments

References

1. Hohmann U, Lau K & Hothorn M The structural basis of ligand perception and signal activation by receptor kinases. Annu. Rev. Plant Biol 68, 109–137 (2017). [PubMed: 28125280]

2. Ma X, Xu G, He P & Shan L SERKing Coreceptors for Receptors. Trends Plant Sci. 21, 1017–1033 (2016). [PubMed: 27660030]

3. Chinchilla D et al. A flagellin-induced complex of the receptor FLS2 and BAK1 initiates plant defence. Nature 448, 497–500 (2007). [PubMed: 17625569]

4. Heese A et al. The receptor-like kinase SERK3/BAK1 is a central regulator of innate immunity in plants. Proc. Natl Acad. Sci. USA 104, 12217–12222 (2007). [PubMed: 17626179]

5. Roux M et al. The Arabidopsis leucine-rich repeat receptor-like kinases BAK1/SERK3 and BKK1/ SERK4 are required for innate immunity to hemibiotrophic and biotrophic pathogens. Plant Cell 23, 2440–2455 (2011). [PubMed: 21693696]

6. Nam KH & Li J BRI1/BAK1, a receptor kinase pair mediating brassinosteroid signaling. Cell 110, 203–212 (2002). [PubMed: 12150928]

7. Li J et al. BAK1, an Arabidopsis LRR receptor-like protein kinase, interacts with BRI1 and modulates brassinosteroid signaling. Cell 110, 213–222 (2002). [PubMed: 12150929]

8. Sun Y et al. Structure reveals that BAK1 as a co-receptor recognizes the BRI1-bound brassinolide. Cell Res. 23, 1326–1329 (2013). [PubMed: 24126715]

9. Wang X et al. Sequential transphosphorylation of the BRI1/BAK1 receptor kinase complex impacts early events in brassinosteroid signaling. Dev. Cell 15, 220–235 (2008). [PubMed: 18694562]

10. Karlova R et al. Identification of in vitro phosphorylation sites in the Arabidopsis thaliana somatic embryogenesis receptor-like kinases. Proteomics 9, 368–379 (2009). [PubMed: 19105183]

11. Yun et al. Analysis of phosphorylation of the BRI1/BAK1 complex in Arabidopsis reveals amino acid residues critical for receptor formation and activation of BR signaling. Mol. Cells 27, 183–190 (2009). [PubMed: 19277500]

12. Wu X et al. Transphosphorylation of E. coli proteins during production of recombinant protein kinases provides a robust system to characterize kinase specificity. Front. Plant Sci 3, 262 (2012). [PubMed: 23226150]

13. Yan L et al. Structural basis for the impact of phosphorylation on the activation of plant receptor-like kinase BAK1. Cell Res. 22, 1304–1308 (2012). [PubMed: 22547027]

14. Ntoukakis V, Schwessinger B, Segonzac C & Zipfel C Cautionary notes on the use of C-terminal BAK1 fusion proteins for functional studies. Plant Cell 23, 3871–3878 (2011). [PubMed: 22129600]

15. Yu X, Feng B, He P & Shan L From chaos to harmony: responses and signaling upon microbial pattern recognition. Annu. Rev. Phytopath 55, 109–137 (2017).

16. Schwessinger B et al. Phosphorylation-dependent differential regulation of plant growth, cell death, and innate immunity by the regulatory receptor-like kinase BAK1. PLoS Genet. 7, e1002046 (2011). [PubMed: 21593986]

17. Aan den Toorn M, Albrecht C & de Vries S On the Origin of SERKs: bioinformatics analysis of the somatic embryogenesis receptor kinases. Mol. Plant 8, 762–782 (2015). [PubMed: 25864910]

18. Wu D, Liu Y, Xu F & Zhang Y Differential requirement of BAK1 C-terminal tail in development and immunity. J. Integr. Plant Biol, doi:10.1111/jipb.12623 (2017).

19. Macho AP, Lozano-Durán R & Zipfel C Importance of tyrosine phosphorylation in receptor kinase complexes. Trends Plant Sci. 20, 269–272 (2015). [PubMed: 25795237]

20. Wang Y et al. Assessment of BAK1 activity in different plant receptor-like kinase complexes by quantitative profiling of phosphorylation patterns. J. Proteomics 108, 484–493 (2014). [PubMed: 24953020]

21. Macho AP et al. A Bacterial tyrosine phosphatase inhibits plant pattern recognition receptor activation. Science 343, 1509–1512 (2014). [PubMed: 24625928]

22. Mitra SK et al. An autophosphorylation site database for leucine-rich repeat receptor-like kinases in Arabidopsis thaliana. Plant J. 82, 1042–1060 (2015). [PubMed: 25912465]

23. Bender KW et al. Glutaredoxin AtGRXC2 catalyses inhibitory glutathionylation of Arabidopsis BRI1-associated receptor-like kinase 1 (BAK1) in vitro. Biochem. J 467, 399–413 (2015). [PubMed: 25678081]

24. Meng X et al. Ligand-induced receptor-like kinase complex regulates floral organ abscission in Arabidopsis. Cell Rep. 14, 1330–1338 (2016). [PubMed: 26854226]

25. Meng X et al. Differential function of Arabidopsis SERK family receptor-like kinases in stomatal patterning. Curr. Biol 25, 2361–2372 (2015). [PubMed: 26320950]

26. Stührwohldt N, Dahlke RI, Steffens B, Johnson A & Sauter M Phytosulfokine-α controls hypocotyl length and cell expansion in Arabidopsis thaliana through phytosulfokine receptor 1. PloS One 6, e21054 (2011). [PubMed: 21698171]

27. Shpak ED, Berthiaume CT, Hill EJ & Torii KU Synergistic interaction of three ERECTA-family receptor-like kinases controls Arabidopsis organ growth and flower development by promoting cell proliferation. Development 131, 1491–1501 (2004). [PubMed: 14985254]

28. Suzuki M et al. Autophosphorylation of specific threonine and tyrosine residues in Arabidopsis CERK1 is essential for the activation of chitin-induced immune signaling. Plant Cell Physiol. 57, 2312–2322 (2016). [PubMed: 27565204]

29. Zhang G et al. Mass spectrometry mapping of epidermal growth factor receptor phosphorylation related to oncogenic mutations and tyrosine kinase inhibitor sensitivity. J. Prot. Res 10, 305–319 (2011).

30. Singh V et al. Tyrosine-610 in the receptor kinase BAK1 does not play a major role in brassinosteroid signaling or innate immunity. Front. Plant Sci 8, doi:10.3389/fpls.2017.01273 (2017).

31. Robatzek S, Chinchilla D & Boller T Ligand-induced endocytosis of the pattern recognition receptor FLS2 in Arabidopsis. Genes Dev. 20, 537–542 (2006). [PubMed: 16510871]

32. Nekrasov V et al. Control of the pattern-recognition receptor EFR by an ER protein complex in plant immunity. EMBO J. 28, 3428–3438 (2009). [PubMed: 19763086]

33. Lee JS et al. Direct interaction of ligand–receptor pairs specifying stomatal patterning. Genes Dev. 26, 126–136 (2012). [PubMed: 22241782]

34. Clough SJ & Bent AF Floral dip: a simplified method for Agrobacterium-mediated transformation ofArabidopsis thaliana. Plant J. 16, 735–743 (1998). [PubMed: 10069079]

35. Kadota Y et al. Direct regulation of the NADPH oxidase RBOHD by the PRR-associated kinase BIK1 during plant immunity. Mol. Cell 54, 43–55 (2014). [PubMed: 24630626]

36. Felix G, Duran JD, Volko S & Boller T Plants have a sensitive perception system for the most conserved domain of bacterial flagellin. Plant J. 18, 265–276 (1999). [PubMed: 10377992]

37. Huffaker A, Pearce G & Ryan CA An endogenous peptide signal in Arabidopsis activates components of the innate immune response. Proc. Natl Acad. Sci. USA 103, 10098–10103 (2006). [PubMed: 16785434]

38. Kunze G et al. The N terminus of bacterial elongation factor Tu elicits innate immunity in Arabidopsis plants. Plant Cell 16, 3496–3507 (2004). [PubMed: 15548740]

39. Monaghan J et al. The calcium-dependent protein kinase CPK28 buffers plant immunity and regulates BIK1 turnover. Cell Host Microbe 16, 605–615 (2014). [PubMed: 25525792]

40. Yoo S-D, Cho Y-H & Sheen J Arabidopsis mesophyll protoplasts: a versatile cell system for transient gene expression analysis. Nat. Protocols 2, 1565–1572 (2007). [PubMed: 17585298]

41. Sun Y et al. Structural basis for flg22-induced activation of the Arabidopsis FLS2-BAK1 immune complex. Science 342, 624–628 (2013). [PubMed: 24114786]

42. Ladwig F et al. Phytosulfokine regulates growth in Arabidopsis through a response module at the plasma membrane that includes CYCLIC NUCLEOTIDE-GATED CHANNEL17, H^+-ATPase, and BAK1. Plant Cell 27, 1718–1729 (2015). [PubMed: 26071421]

43. Bender KW et al. Autophosphorylation-based calcium (Ca2+) sensitivity priming and Ca2+/calmodulin inhibition of Arabidopsis thaliana Ca2+-dependent protein kinase 28 (CPK28). J. Biol. Chem 292, 3988–4002 (2017). [PubMed: 28154194]

44. Horst RJ et al. Molecular framework of a regulatory circuit initiating two-dimensional spatial patterning of stomatal lineage. PLoS Gen. 11, e1005374 (2015).

45. Holm L & Laakso LM Dali server update. Nucleic acids research 44, W351–355 (2016). [PubMed: 27131377]

46. Lehti-Shiu MD & Shiu S-H Diversity, classification and function of the plant protein kinase superfamily. Philos. Trans. Royal Soc. B 367, 2619–2639 (2012).

47. Shiu SH & Bleecker AB Receptor-like kinases from Arabidopsis form a monophyletic gene family related to animal receptor kinases. Proc. Natl Acad. Sci. USA 98, 10763–10768 (2001). [PubMed: 11526204]
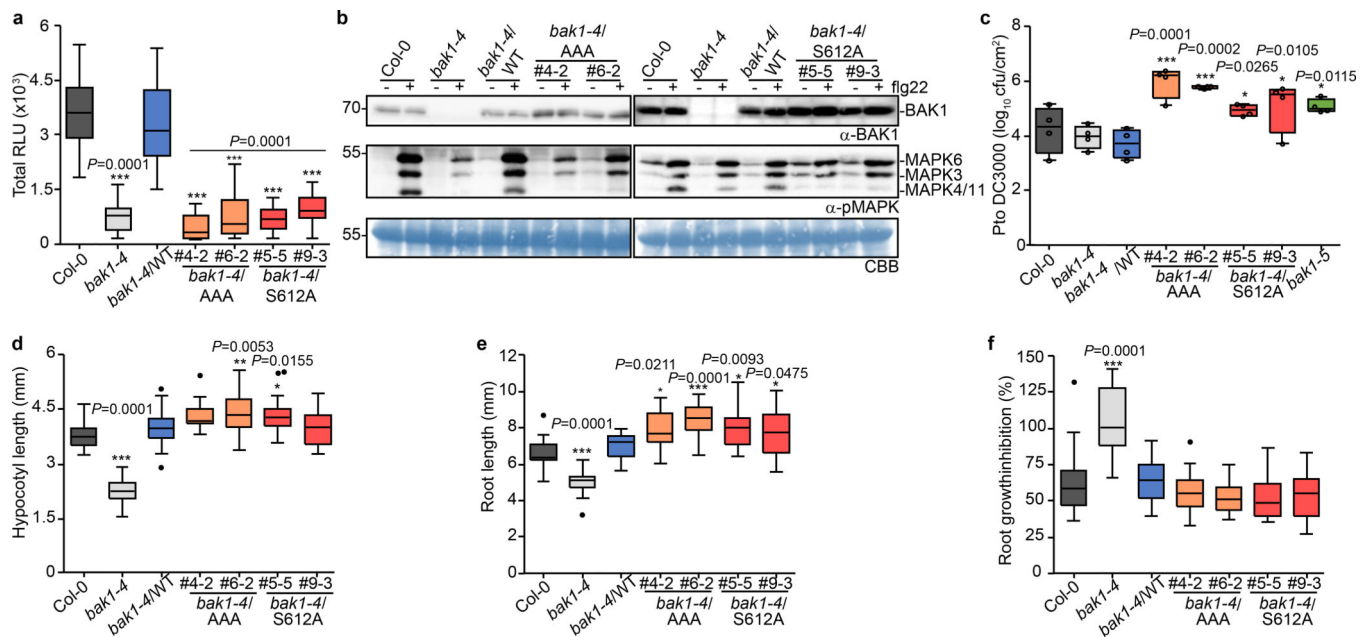
Figure 1 |. Phosphorylation of the BAK1 C-terminal tail is critical for immune signaling.
a, Total ROS production following treatment (n=12 biologically independent leaf discs) with 100 nM flg22 over 60 min. RLU, relative luminescence unit. **b**, MAP kinase activation 5 min after treatment of 10-day-old seedlings with 100 nM flg22. Coomassie brilliant blue (CBB) was used as loading control. For blot source data, see Supplementary Figure 1. **c**, Growth of *Pto* DC3000 at 3 days post-inoculation. Plants were sprayed with a 10^8 cfu/mL bacterial suspension. n=4 biologically independent plants. Circles indicate the individual data points. **d**, Hypocotyl length of dark-grown 7-day-old seedlings grown on medium supplemented with 2 μM BRZ. Biologically independent hypocotyls: Col-0 (n=19), *bak1–4* (n=27), *bak1–4/*WT (n=28), *bak1–4/*AAA#4–2 (n=18), *bak1–4/*AAA#6–2 (n=22), *bak1–4/* S612A#5–5 (n=33), *bak1–4/*S612A#9–3 (n=29) **e**, Root length of light-grown 7-day-old seedlings grown on medium supplemented with 2 μM BRZ. Biologically independent roots: Col-0 (n=21), *bak1–4* (n=21), *bak1–4/*WT (n=21), *bak1–4/*AAA#4–2 (n=25), *bak1–4/* AAA#6–2 (n=27), *bak1–4/*S612A#5–5 (n=24), *bak1–4/*S612A#9–3 (n=25) **f**, Relative root growth inhibition of light-grown 7-day-old seedlings treated with 5 nM BL. Control and treated media were supplemented with 0.5 μM BRZ. Root length growth inhibition by BL was calculated relative to the untreated control for each genotype for the following numbers of biologically independent roots: Col-0 (n= 17), *bak1–4* (n= 23), *bak1–4/*WT (n=24), *bak1– 4/*AAA#4–2 (n=25), *bak1–4/*AAA#6–2 (n=27), *bak1–4/*S612A#5–5 (n=22), *bak1–4/* S612A#9–3 (n=23). **a-f,** Experiments were repeated independently three times. Measurements are plotted as boxplots displaying the first and third quartiles, split by the median; whiskers extend to a maximum of 1.5 × interquartile range beyond the box. Outliers are indicated as black dots. Statistical analysis was performed using one-way ANOVA with Dunnett's post-hoc test compared to the *bak1–4/*WT.
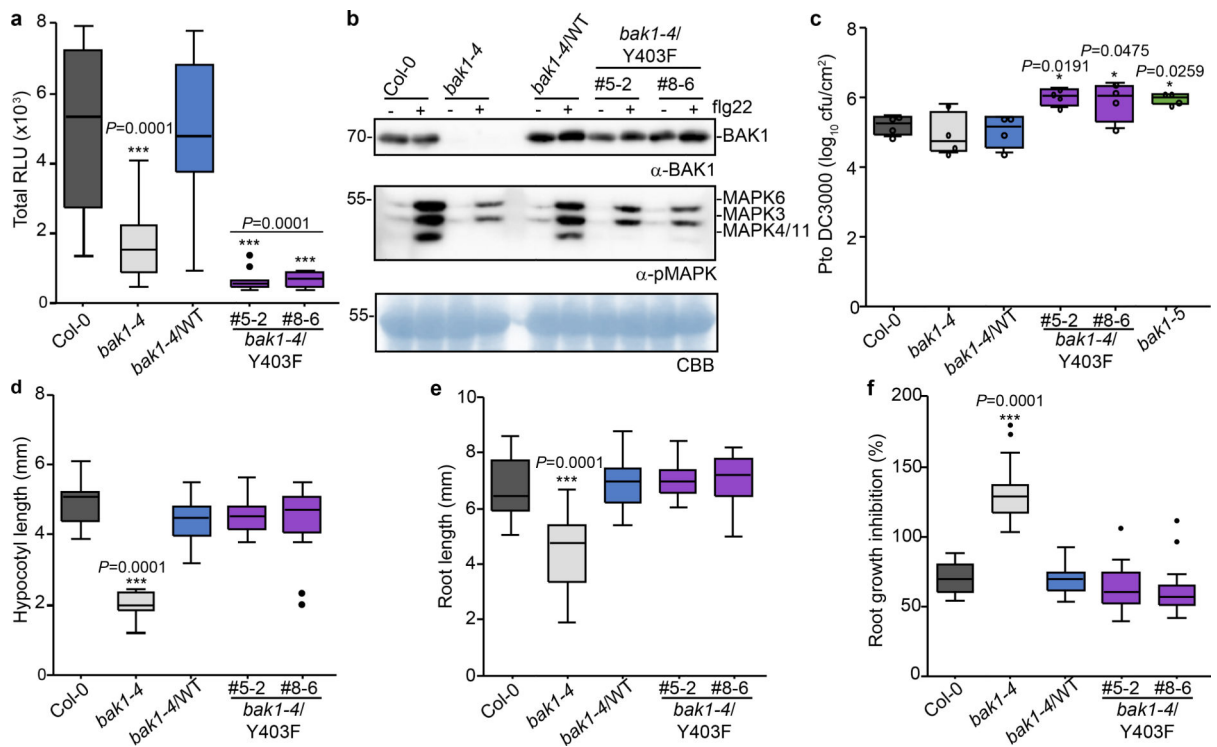
Figure 2 |. Phosphorylation of Tyr403 is required for BAK1 function in immune signaling.
a, Total ROS production following treatment (n=12 biologically independent leaf discs) with
100 nM flg22 over 60 min. **b**, MAP kinase activation 5 min after treatment of 10-day-old
seedlings with 100 nM flg22. Coomassie brilliant blue (CBB) was used as loading control.
For blot source data, see Supplementary Figure 1. **c**, Growth of *Pto* DC3000 bacteria 3 days
post-inoculation. Plants were sprayed with a 10^8 cfu/mL bacterial suspension. n=4
biologically independent plants. Circles indicate the individual data points. **d**, Hypocotyl
length of dark-grown 7-day-old seedlings grown on medium supplemented with 2 μM BRZ.
Biologically independent hypocotyls: Col-0 (n= 15), *bak1–4* (n= 13), *bak1–4/*WT (n=15),
*bak1–4/*Y403F#5–2 (n=22), *bak1–4/*Y403F#8–6 (n=22). **e**, Root length of light-grown 7-
day-old seedlings grown on medium supplemented with 2 μM BRZ. Biologically
independent roots: Col-0 (n= 17), *bak1–4* (n= 18), *bak1–4/*WT (n=17), *bak1–4/*Y403F#5–2
(n=20), *bak1–4/*Y403F#8–6 (n=23). **f**, Relative root growth inhibition of light-grown 7-day-
old seedlings treated with 5 nM BL. Control and treated media were supplemented with 0.5
μM BRZ. Root length growth inhibition by BL was calculated relative to the untreated
control for each genotype, for the following numbers of biologically independent roots:
Col-0 (n= 19), *bak1–4* (n= 23), *bak1–4/*WT (n=17), *bak1–4/*Y403F#5–2 (n=18), *bak1–4/*
Y403F#8–6 (n=20). **a-f,** experiments were repeated independently three times.
Measurements are plotted as boxplots displaying the first and third quartiles, split by the
median; whiskers extend to a maximum of 1.5 × interquartile range beyond the box. Outliers
are indicated as black dots. Statistical analysis was performed using one-way ANOVA with
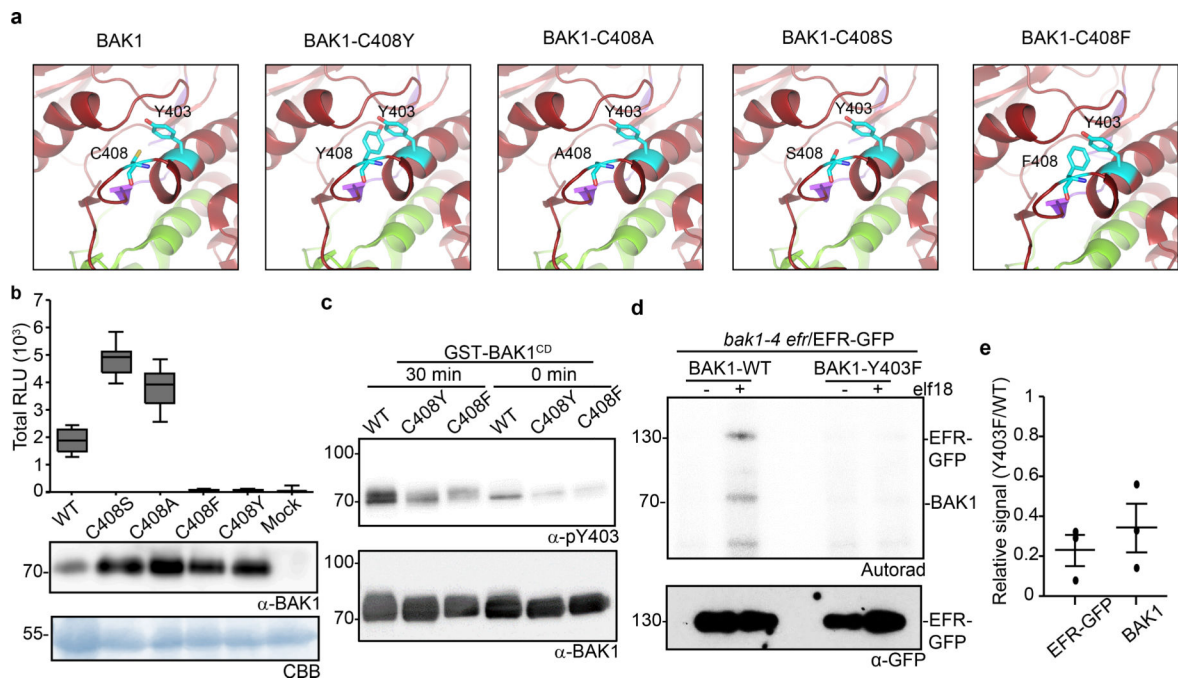Dunnett's post-hoc test compared to the *bak1–4/*WT.

Figure 3 |. Phosphorylation of the conserved BAK1-Tyr403 residue is important for ligand-induced activation of immune receptor complex.

a, *In silico* substitutions of BAK1-C408 on a selected region of the BAK1 cytoplasmic domain (BAK1^{CD}) structure (3UIM.pdb). The activation segment (green) and catalytic loop (purple) are highlighted. **b**, Total ROS production following treatment with 100 nM flg22 over 60 min of n=12 biological independent suspensions of *bak1–4* mesophyll protoplasts transiently expressing the indicated BAK1 mutants. Measurements are plotted as boxplots displaying the first and third quartiles, split by the median; whiskers extend to a maximum of $1.5 \times$ interquartile range beyond the box. **c**, *In vitro* Y403 phosphorylation of recombinant BAK1^{CD} proteins after a 30-minute kinase reaction as detected by α-pY403. Blots were further probed with α-BAK1 for loading control. **b, c,** Experiments were repeated independently three times. **d**, Phosphorylation of EFR-GFP and associated BAK1 after treatment with water (–) or 100 nM elf18 (+) for 10 min. EFR-GFP was immuno-precipitated using GFP-Trap beads and then submitted to an *in vitro* kinase assay with [^{32}P]γ-ATP. EFR-GFP levels were determined by western blot analysis with α-GFP antibodies. **b-d,** For gel source data, see Supplementary Figure 1. **e**, Aligned dot blots show the relative reductions in BAK1 and EFR-GFP phosphorylation levels in the *bak1–4/*Y403F/EFR-GFP sample, as measured in three independent experiments of *in vitro* kinase assays as in (**d**). Line represent mean and error bar SE.
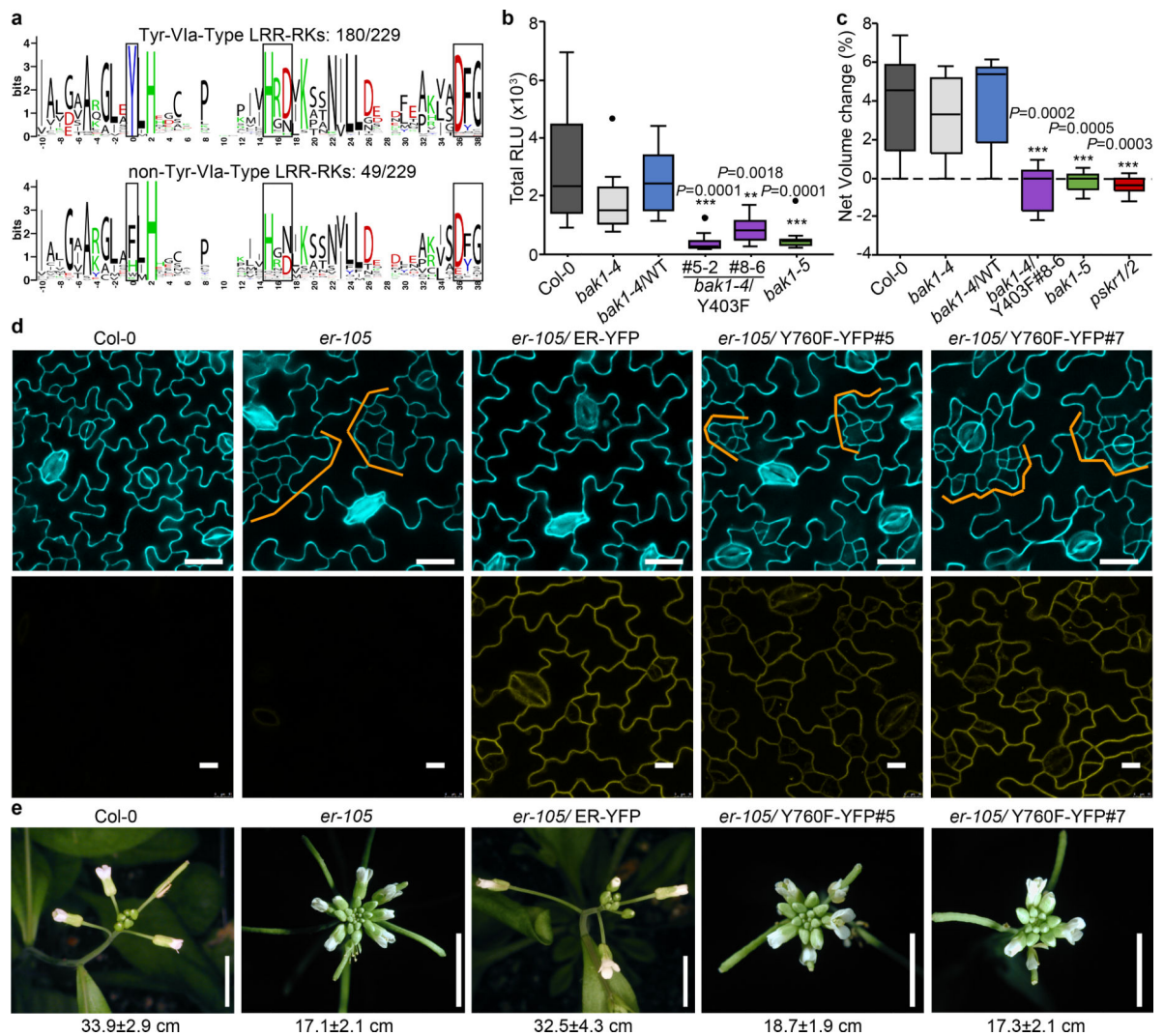
Figure 4 |. BAK1-Tyr403 and analogous Tyr phosphorylation plays a wide functional role for Arabidopsis LRR-RKs.

a, WebLogo representation of the region analogous BAK1-Y403 in Arabidopsis LRR-RKs.
b, Total ROS production following treatment of n=12 biologically independent leaf discs with 100 nM Pep1 over 60 min. **c**, Cell expansion of mesophyll protoplasts (as measured by net volume change) following treatment with 1 nM PSK-α (n=10 biologically independent protoplasts). **b, c,** Measurements are plotted as boxplots displaying the first and third quartiles, split by the median; whiskers extend to a maximum of 1.5 × interquartile range beyond the box. Outliers are indicated as black dots. Statistical analysis was performed using one-way ANOVA and Dunnett's post-hoc test compared to the *bak1–4/*WT. **d**, Confocal images of abaxial cotyledon epidermis. Top panel, epidermal phenotypes from 10-day-old seedlings. Cell outlines are visualized with propidium iodide staining; bottom panel, ER-YFP expression from 3-day-old seedlings. **e**, Representative images of inflorescence from 4- to 5-week-old plants. Scale bars, 5 mm. The main inflorescence lengths from n= 11 (Col-0), n=18 (*er-105*), n=8 (*er-105*/ER-YFP), n=19 (*er-105*/Y760F-YFP #5) and n=19 (*er-105*/Y760F-YFP #5) biologically independent plants (7-week-old) were measured. Mean

±SEM values are indicated below the image panels. **b-e,** Experiments were repeated at least twice with similar results.

HHMI Author Manuscript

HHMI Author Manuscript

HHMI Author Manuscript